

Effects of electroweak radiative corrections in polarized low-energy electron-positron annihilation into lepton pairs

A. Arbuzov¹, S. Bondarenko¹, Ya. Dydyshka^{2,3}, L. Kalinovskaya²,
L. Rumyantsev², R. Sadykov², V. Yermolchyk^{2,3}, and U. Yermolchyk^{2,3}

¹Bogoliubov Laboratory of Theoretical Physics, JINR, 141980 Dubna, Moscow region, Russia

²Dzhelepov Laboratory of Nuclear Problems, JINR, 141980 Dubna, Moscow region, Russia

³Institute for Nuclear Problems, Belarusian State University, Minsk, 220006 Belarus

June 22, 2022

Abstract

Complete one-loop electroweak radiative corrections to the cross section of the process $e^+e^- \rightarrow \mu^-\mu^+(\tau^-\tau^+)$ are evaluated with the help of the **SANC** system. Higher-order contributions of the initial state radiation are computed in the QED structure function formalism. Numerical results are given for the center-of-mass energy range $\sqrt{s} = 5, 7$ GeV for various polarization degrees of the initial particles.

1 Introduction

Processes of electron-positron annihilation provide a powerful tool in studies of elementary particles. In particular, modern e^+e^- colliders, such as VEPP-2000 (Novosibirsk), BEPC II (Beijing), KEKB (Tsukuba) etc., are well suited for production and high-precision studies of hadrons. Electron-positron colliders have significant advantages: clean signals, a low background, a high efficiency and resolution. The continuously increasing experimental accuracy challenges the theory to provide more and more precise predictions. For example, the current and upcoming experiments SuperKEKB [1], BES-III [2], Super Charm-Tau Factory [3] and Super Tau-Charm Facility [4] aim at reaching an error of a few per mille in luminosity measurements. This requires new calculations with taking into account higher order perturbative corrections and other effects including electroweak ones.

Another important advantage of e^+e^- colliders is the possibility of using polarized beams. Several future projects of such machines foresee having at least longitudinally polarized electron beams. That will open new possibilities in high-precision studies of the charm quark and tau lepton physics. A very high accuracy of checking the universality of the neutral current vector couplings and in searches for CP-violation in the lepton sector will be achieved. A new independent measurement of the effective electroweak mixing parameter $\sin^2\theta_W$ through left-right asymmetries will be complementary to the corresponding studies at higher energies. Measurements with polarized beams will also help to refine the elements of the Cabibbo-Kobayashi-Maskawa matrix, study QCD at low energies and exotic hadrons, search for new physics and extensively investigate two-photon physics. The SuperKEKB team (Belle collaboration) [5] considers plans of an upgrade to have longitudinally polarized electron beam [6, 7]. That will significantly widen the collider's capability of examining the electroweak sector.

BES-III has collected more than 35 fb^{-1} of integrated luminosity at different center-of-mass system (c.m.s.) energies from 2.0 to 4.94 GeV. The upgrade of BES-III will increase the peak luminosity by a factor of 3 for beam energies from 2.0 to 2.8 GeV (CM energies from 4.0 to 5.6 GeV). Future Super Charm-Tau Factories (Super Charm-Tau Factory project [3] and High Intensity Electron Positron Advanced Facility (HIEPAF) [4]) are accelerator complexes for high-precision measurements between 2 and 5(7) GeV with luminosity up to $10^{35}\text{ cm}^{-2}\text{ s}^{-1}$ and longitudinal polarization. They will deliver up to 1 ab^{-1} of integrated luminosity per year.

In connection with these challenges, one of the most demanded processes is the lepton pair production (LPP) both for estimating luminosity and for physics program. Various experimental facilities operating at low energies are in plans or already in action demanding appropriate software for theoretical predictions. At the moment, the most advanced and widely used generators with one-loop radiative corrections (RC) for estimation of LPP at low energies are **BabaYaga** [8, 9, 10, 11], **KKMC** [12, 13], and **MCJPG** [14]. Recently, a new Monte-Carlo generator [15] for the simulation of lepton pair productions and τ lepton decays up to an energy of about 11 GeV has been presented.

The **SANC** Monte Carlo event generator **ReneSANCe** [16] and integrator **MCSANCee** are relatively new software tools. They can be used in the mentioned energy domain of electron-positron colliders for simulation of LPP and Bhabha processes. These tools provide the possibility of evaluating the complete one-loop QED and (electro)weak radiative corrections. Some higher-order leading corrections are also implemented. In addition, the tools produce results in the full phase space and also allow taking into account longitudinal beam polarizations. To match the high precision of current and near-future experiments we plan to implement also higher-order next-to-leading QED radiative corrections.

In this article, we analyze the effects due to electroweak RC and polarization of the colliding beams using the **SANC** software. We consider the processes of electron-positron annihilation into a lepton pair

$$e^+(p_1, \chi_1) + e^-(p_2, \chi_2) \rightarrow l^-(p_3, \chi_3) + l^+(p_4, \chi_4)(+\gamma(p_5, \chi_5)), \quad (1)$$

where $l = \mu, \tau$ with allowance for arbitrary longitudinal polarization of the initial particles (χ_i correspond to the helicities of the particles). We keep in mind experiments at relatively low c.m.s. energies up to about 7 GeV which is relevant for the Super Charm-Tau Factory. Our aim is to analyze the size of different RC contributions, estimate the resulting theoretical uncertainty, and verify the necessity to include other higher-order corrections.

The article is organized as follows. In Section 2, we discuss various contributions to the cross sections. In Section 3, the corresponding numerical results are given for the total and differential cross sections. We consider in detail all possible contributions to the cross sections at c.m.s. energies of $\sqrt{s} = 5$ and 7 GeV. Numerical results are obtained by an estimate of polarization effects. In Section 4, we analyze the results.

2 The state-of-the-art radiative corrections at low energies in SANC

For a detailed analysis, we divide the contributions to the full correction into several parts: the Born level cross section, electroweak (EW) corrections, contribution from vacuum polarization, and multiple photon emission effects.

Born level

We evaluate the Born level cross section (leading order, LO) contribution for two cases: 1) with pure photon exchange $\sigma_{\text{QED}}^{\text{Born}}(\gamma)$ and 2) with both photon and Z boson exchange $\sigma_{\text{QED}}^{\text{Born}}(\gamma, Z)$.

Electroweak corrections

We have already described in detail the technique and results of the analytic calculations of the scalar form factors and helicity amplitudes of the general LPP process (1) in our recent paper [17]. For EW corrections, we calculate the following contributions and introduce the notation for them:

- QED level

Gauge invariant subsets of QED corrections are evaluated separately, i.e., the initial state radiation (ISR), the final state radiation (FSR), and the initial-final interference (IFI).

- Weak and higher order corrections

At low energies, weak-interaction contributions are typically small since they are suppressed by the ratio s/M_Z^2 . But for high-precision measurements they might be still numerically relevant. We have found it appropriate to combine the contributions of the same order of smallness, i.e., weak and higher-order corrections. The corresponding relative contributions will be further denoted as δ^{weak} and δ^{ho} . We also distinguish here two possibilities: 1) the complete one-loop δ^{weak} , where pure weak-interaction and vacuum polarization (VP) contributions are

taken into account¹; and 2) the pure weak-interaction contribution $\delta^{\text{weak-VP}} = \delta^{\text{weak}} - \delta^{\text{VP}}$.

We evaluate the leading higher-order EW corrections δ^{ho} to four-fermion processes through the $\Delta\alpha$ and $\Delta\rho$ parameters. A detailed description of our implementation of this contribution was presented in [18].

Vacuum polarization

We introduce two options to account for the contribution of vacuum polarization: δ_1^{VP} is the choice of hadronic vacuum polarization $\Delta\alpha_{\text{had}}^{(5)}(M_Z)$ part using a parametrization with auxiliary quarks masses; and δ_2^{VP} is the choice using public versions of the **AlphaQED** code by F. Jegerlehner [19].

Multiple photon effects

The implementation into **SANC** of the multiple photon effects, i.e. ISR (FSR) corrections in the leading logarithmic approximation (LLA) through the apparatus of QED structure functions [20, 21] which was described in detail in [22]. Results are shown up to $\mathcal{O}(\alpha^3 L^3)$ finite terms for an exponentiated representation and up to $\mathcal{O}(\alpha^4 L^4)$ for order-by-order calculations. The corresponding relative corrections are denoted below as $\delta^{\text{LLA,ISR(FSR,IFI)}}$.

Particular contributions to ISR(FSR) are sensitive to experimental cuts. Our cuts are appropriate to the conditions of the Super Charm-Tau Factory project.

The master formula for a general e^+e^- annihilation cross section with ISR QED corrections in the leading logarithmic approximation has the same structure as the one for the Drell-Yan process. For ISR corrections in the annihilation channel, the large logarithm is $L = \ln(s/m_e^2)$ where the total c.m.s. energy \sqrt{s} is chosen as the factorization scale.

In the LLA approximation we separate the pure photonic corrections (marked “ γ ”) and the remaining ones which include the pure pair and mixed photon-pair effects (marked “ e^+e^- ” or $\mu^+\mu^-$). Here we do not consider the correction due to light hadron pairs. Numerically, it is comparable with the muon pair contribution but strongly depends on the event selection procedure. So, the corrections due to hadronic effects will be treated elsewhere. The corresponding relative corrections are denoted as $\delta^{\text{LLA},i}(k)$ with $i = \text{ISR, FSR, IFI}$, and k suggests the correction type: γ , e^+e^- pairs, or $\mu^+\mu^-$ pairs.

3 Numerical results and comparisons

In this section, we show numerical results for electroweak radiative corrections to the annihilation process (1) obtained by means of the **SANC** system. Numerical results contain estimates of polarization effects. We compute total cross sections as well as angular distributions at the one-loop level.

¹Inclusion of the vacuum polarization contribution into the *weak* subset of corrections is natural in **SANC** since the latter is a part of electroweak form factors.

Here we used the following set of input parameters:

$$\begin{aligned}
\alpha^{-1}(0) &= 137.035999084, \\
M_W &= 80.379 \text{ GeV}, \quad M_Z = 91.1876 \text{ GeV}, \\
\Gamma_Z &= 2.4952 \text{ GeV}, \quad m_e = 0.51099895000 \text{ MeV}, \\
m_\mu &= 0.1056583745 \text{ GeV}, \quad m_\tau = 1.77686 \text{ GeV}, \\
m_d &= 0.083 \text{ GeV}, \quad m_s = 0.215 \text{ GeV}, \\
m_b &= 4.7 \text{ GeV}, \quad m_u = 0.062 \text{ GeV}, \\
m_c &= 1.5 \text{ GeV}, \quad m_t = 172.76 \text{ GeV}.
\end{aligned} \tag{2}$$

The angular cuts are applied to the final state leptons:

$$|\cos \theta_{\mu-}| < 0.9, \quad |\cos \theta_{\mu+}| < 0.9, \tag{3}$$

where $\theta_{\mu\pm}$ are angles with respect to the beam axis.

All calculations are done in the $\alpha(0)$ EW scheme in order to have a direct access to the effect of vacuum polarization. In this scheme, the fine structure constant $\alpha(0)$ and all particle masses are input parameters. All the results are obtained for the c.m.s. energies $\sqrt{s} = 5$ and 7 GeV and for the following three sets of magnitudes of the electron (P_{e-}) and positron (P_{e+}) beam polarizations:

$$(P_{e-}, P_{e+}) = (0, 0), (-0.8, 0), (0.8, 0). \tag{4}$$

3.1 Different radiative correction contributions

In order to quantify the impact of different contributions, we divide them into several parts: three gauge-invariant subsets of QED one-loop corrections, the vacuum polarization contribution, the weak interaction effects, and the higher order LLA QED contributions. The three QED RC subsets are due to the initial state radiation (ISR), the final state radiation (FSR), and the interference of the initial and final state radiation (IFI).

The corresponding results for the total LPP cross section are presented in Table 1, where the relative corrections δ^i are computed as the ratios (in percent) of the corresponding RC contributions to the Born level cross section. Table 2 illustrates the size of the ISR higher-order QED corrections computed within the collinear leading logarithmic approximation.

In the upper panel of Figure 1, the Born cross section and the corrected one which includes the EW NLO and higher-order corrections are shown as a function of the initial c.m.s. energy ($\sqrt{s} = 2 - 12$ GeV) of the electron and positron beams. The cross sections show the fast drop from the ~ 20 nanobarn at the c.m.s energy $\sqrt{s} = 2$ GeV to about one-half of a picobarn at $\sqrt{s} = 12$ GeV.

In the lower panel of Figure 1 the relative corrections to the Born cross section are shown in parts, namely, the pure QED, vacuum polarization (VP) and EW higher-order contributions.

Table 1: Integrated Born and one-loop cross sections and relative corrections for the $e^+e^- \rightarrow \mu^-\mu^+(\gamma)$ process at the c.m.s. energies $\sqrt{s} = 5$ and 7 GeV in the $\alpha(0)$ EW scheme with angular cuts 3.

\sqrt{s} , GeV	5	7
σ^{Born} , pb	2978.58(1)	1519.55(1)
$\delta^{\text{weak-VP}}$, %	0.029(1)	0.005(1)
δ_1^{VP} , %	5.467(1)	6.272(1)
δ_2^{VP} , %	5.430(1)	6.250(1)
δ^{ho} , %	0.224(1)	0.294(1)
$\delta^{\text{QED, ISR}}$, %	8.455(2)	9.063(1)
$\delta^{\text{QED, FSR}}$, %	-0.016(1)	-0.014(1)
$\delta^{\text{QED, IFI}}$, %	0.012(2)	0.017(1)
$\delta^{\text{LLA, ISR}}$, %	0.668(1)	0.850(1)
$\delta^{\text{LLA, FSR}}$, %	0.047(1)	0.070(1)

Table 2: Higher-order ISR corrections in the LLA approximation for the $e^+e^- \rightarrow \mu^-\mu^+(n\gamma)$ process at $\sqrt{s} = 5$ and 7 GeV with cuts 3. Here $\delta_{\text{ISR LLA}} \equiv \delta\sigma_{\text{ISR LLA}}/\sigma_0 \times 100\%$.

	δ , %	
\sqrt{s} , GeV	5	7
$\mathcal{O}(\alpha^2 L^2)$, γ	0.315(1)	0.436(1)
$\mathcal{O}(\alpha^2 L^2)$, e^+e^-	0.238(1)	0.258(1)
$\mathcal{O}(\alpha^2 L^2)$, $\mu^+\mu^-$	0.100(1)	0.114(1)
$\mathcal{O}(\alpha^3 L^3)$, γ	-0.008(1)	-0.004(1)
$\mathcal{O}(\alpha^3 L^3)$, e^+e^-	0.016(1)	0.033(1)
$\mathcal{O}(\alpha^3 L^3)$, $\mu^+\mu^-$	0.007(1)	0.015(1)

The main impact is due to the QED effects, being from 5% to 10 %. The vacuum polarization contribution is also large, ranging from 4% to 8%. The contribution of higher order is proportional to α^n ($n \geq 2$) and makes up about 0.1 – 0.4 % because of being enhanced by large logarithms. Vacuum polarization is treated in two ways. In the first one, the hadronic part of vacuum polarization is parameterized by auxiliary quarks masses (it is marked “VP₁” on the plot). In the second one, we use the parameterization by F. Jegerlehner which accounts for hadron resonances [19] (it is marked “VP₂” on the plot). In both cases, leptonic contributions are taken into account. One can see that the two parameterizations agree well at higher energies in regions without resonance. But in general, the second parameterization is more appropriate for the given energy range.

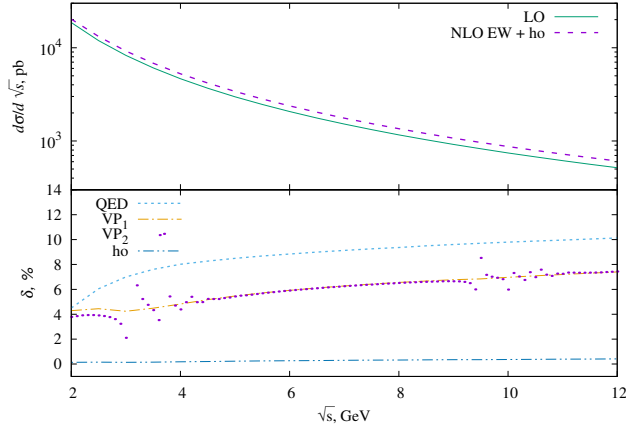


Figure 1: Born level (LO) and corrected (EW NLO + ho) cross sections of the $e^+e^- \rightarrow \mu^-\mu^+(\gamma)$ process for the c.m.s. energy range $\sqrt{s} = 2 - 12$ GeV (upper panel). The relative corrections of the QED, vacuum polarization (VP), and higher-order (ho) contributions (lower panel).

4 Comparison with BabaYaga code

Table 3: Tuned comparison of the Born and QED NLO integrated cross sections produced by the SANC and BabaYaga codes

\sqrt{s} , GeV	5	7
Born, nb		
SANC (Z/γ)	2.9786(1)	1.5195(1)
SANC (only γ)	2.9786(1)	1.5196(1)
BabaYaga	2.9786(1)	1.5196(1)
QED NLO, nb		
SANC (Z/γ)	3.2304(1)	1.6575(1)
SANC (only γ)	3.2287(1)	1.6565(1)
BabaYaga	3.2285(1)	1.6565(1)

In Table 3, we present a tuned comparison of the Born and QED NLO (without VP contribution) integrated cross sections produced by the **SANC** and **BabaYaga** codes. The results are obtained for two c.m.s. energies $\sqrt{s} = 5$ and 7 GeV with the angular cut $|\cos \vartheta_\mu| < 0.9$. Very good agreement within statistical errors of the results produced by two codes is found.

Figures 2 and 3 show the comparison of the **SANC** and **BabaYaga** results produced for two c.m.s. energies $\sqrt{s} = 5$ and 7 GeV. In the upper panels of the figures, the LO and QED NLO differential cross sections as functions of the cosine of the outgoing muon momentum angle

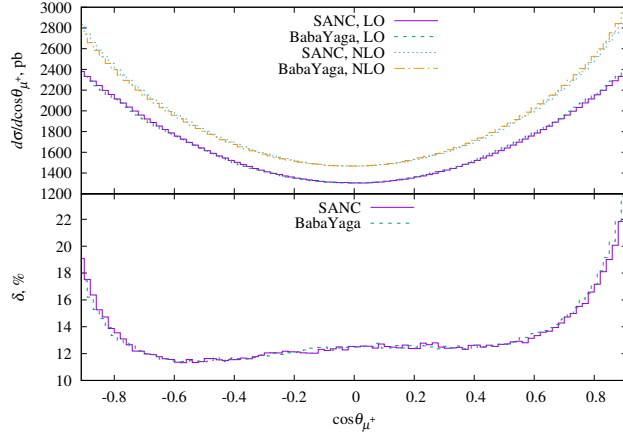


Figure 2: LO and NLO unpolarized pure QED cross sections (upper panel) and the relative corrections (lower panel) produced by the SANC and BabaYaga codes for the c.m.s. energy $\sqrt{s} = 5$ GeV as a function of $\cos\theta_{\mu^+}$.

are shown. In the lower panels the relative corrections are compared. For both c.m.s energies, cross sections and the relative corrections are in good agreement. To obtain the results for Table 3 and Figures 2,3, additional extra efforts were made to exclude the Z boson exchange contribution in the LO and NLO cross sections in the SANC code.

4.1 Polarization dependence of cross sections

Tables 4-6 present the integrated Born and one-loop cross sections in pb and relative corrections in percent for the process $e^+e^- \rightarrow l^-l^+$ at the c.m.s. energy of 5 GeV and set (4) of the initial particle degree of polarization in the $\alpha(0)$ EW scheme. The cases with the 7 GeV c.m.s. energy for the $\mu^+\mu^-$ and $\tau^+\tau^-$ final states are presented in Tables 5 and 7, respectively. It is interesting that the Born and corrected cross sections do depend on beam polarizations while the relative correction is almost constant.

Table 4: Polarized integrated Born cross section and relative corrections for the $e^+e^- \rightarrow \mu^-\mu^+(\gamma)$ scattering for $\sqrt{s} = 5$ GeV for different degree of polarization of the initial particles.

P_{e^+}, P_{e^-}	$\sigma^{\text{Born}}, \text{ pb}$	$\sigma^{\text{1-loop}}, \text{ pb}$	$\delta, \%$
0, 0	2978.6(1)	3434.2(1)	15.30(1)
0, +0.8	2979.1(1)	3434.6(1)	15.29(1)
0, -0.8	2978.0(1)	3433.7(1)	15.30(1)

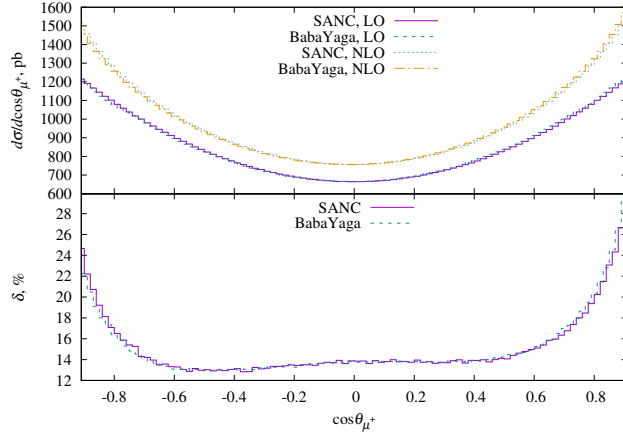


Figure 3: Same as in Figure 2 but for c.m.s. energy $\sqrt{s} = 7$ GeV.

Table 5: Same as in Table 4, but for $\sqrt{s} = 7$ GeV.

P_{e^+}, P_{e^-}	$\sigma^{\text{Born}}, \text{pb}$	$\sigma^{\text{1-loop}}, \text{pb}$	$\delta, \%$
0, 0	1519.6(1)	1773.8(1)	16.73(1)
0, +0.8	1520.1(1)	1774.1(1)	16.71(1)
0, -0.8	1519.0(1)	1773.6(1)	16.76(1)

5 Forward-backward asymmetry

The forward-backward asymmetry A_{FB} is defined as

$$A_{\text{FB}} = \frac{\sigma_{\text{F}} - \sigma_{\text{B}}}{\sigma_{\text{F}} + \sigma_{\text{B}}},$$

$$\sigma_{\text{F}} = \int_0^1 \frac{d\sigma}{d \cos \vartheta_f} d \cos \vartheta_f, \quad \sigma_{\text{B}} = \int_{-1}^0 \frac{d\sigma}{d \cos \vartheta_f} d \cos \vartheta_f, \quad (5)$$

where ϑ_f is the angle between the momenta of the incoming electron and the outgoing negatively charged fermion. It can be measured in any $e^+e^- \rightarrow f\bar{f}$ channels but for precision tests the most convenient channels are $f = e, \mu$.

In Figure 4 we show the behavior of the A_{FB} asymmetry in the Born and 1-loop approximations (with weak, pure QED, or complete EW RC contributions) and of the corresponding ΔA_{FB} for the c.m.s. energy range $2 \leq \sqrt{s} \leq 12$ GeV. The asymmetry in the lowest-order approximation comes from the tree-level Z boson exchange contribution. One can see that for higher energies it is comparable in size with the QED contribution which comes from one-loop radiative corrections.

Table 6: Polarized integrated Born cross section and relative corrections for $e^+e^- \rightarrow \tau^-\tau^+(\gamma)$ scattering for $\sqrt{s} = 5$ GeV.

P_{e^+}, P_{e^-}	$\sigma^{\text{Born}}, \text{ pb}$	$\sigma^{\text{1-loop}}, \text{ pb}$	$\delta, \%$
0, 0	2703.3(1)	2816.7(1)	4.20(1)
0, +0.8	2703.8(1)	2816.9(1)	4.18(1)
0, -0.8	2702.8(1)	2816.5(1)	4.21(1)

Table 7: Same as in Table 6 but for $\sqrt{s} = 7$ GeV.

P_{e^+}, P_{e^-}	$\sigma^{\text{Born}}, \text{ pb}$	$\sigma^{\text{1-loop}}, \text{ pb}$	$\delta, \%$
0, 0	1503.0(1)	1648.8(1)	9.70(1)
0, +0.8	1503.6(1)	1649.1(1)	9.68(1)
0, -0.8	1502.4(1)	1648.5(1)	9.72(1)

6 Conclusions

In this paper, we considered different contributions of EW corrections to processes of electron-positron annihilation into a lepton pair. The corrections were evaluated within the **SANC** system framework in the $\alpha(0)$ EW scheme for c.m.s. energies up to about 10 GeV which are relevant for the existing and future meson factories. The complete one-loop EW corrections as well as some leading higher-order corrections were analyzed. We see that the pure QED and vacuum polarization corrections dominate in the given energy range, but in some cases the Z boson exchange amplitude also becomes numerically relevant. In particular, the latter is visible in the forward-backward asymmetry.

The **SANC** Monte Carlo event generator **ReneSANCe** and integrator **MCSANCee** were used to produce the numerical results. At the one-loop pure QED level for unpolarized beams, good agreement with the corresponding results of the **BabaYaga** code is found. The advantages of our codes is implementation of the complete one-loop (electro)weak corrections and taking into account particle polarizations.

From Table 2 one can see that the second order ISR corrections are numerically relevant for high-precision experiments. That brings us to the conclusion that to reduce the theoretical uncertainty we need to implement the complete two-loop, i.e., $\mathcal{O}(\alpha^2)$ QED corrections, while starting from the third order the corrections can be computed in an approximate manner, i.e., with QED showers or even in the collinear LLA approximation.

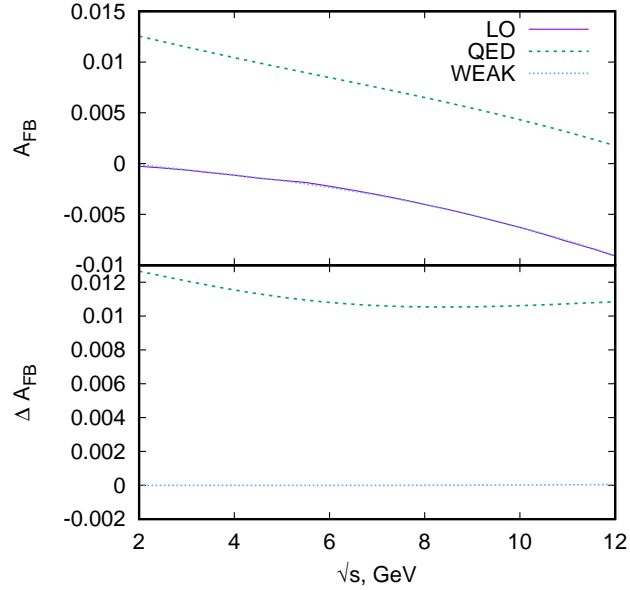


Figure 4: A_{FB} asymmetry in the Born and one-loop approximations and the corresponding shifts ΔA_{FB} for the c.m.s. energy range $\sqrt{s} = 2 - 12$ GeV.

7 Funding

This research was supported by the Russian Foundation for Basic Research, project N 20-02-00441.

8 Acknowledgments

We are grateful to M. Potapov for the help in preparation of the manuscript.

References

- [1] SuperKEKB Collaboration, K. Akai, K. Furukawa, and H. Koiso, *Nucl. Instrum. Meth. A* **907** (2018) 188–199, 1809.01958.
- [2] D. M. Asner *et al.*, *Int. J. Mod. Phys. A* **24** (2009) S1–794, 0809.1869.
- [3] SCTF Collaboration, D. A. Epifanov, *Phys. Atom. Nucl.* **83** (2020), no. 6 944–948.
- [4] H. P. Peng, Y. H. Zheng, and X. R. Zhou, *Physics* **49** (2020), no. 8 513–524.

- [5] Belle-II Collaboration, W. Altmannshofer *et al.*, *PTEP* **2019** (2019), no. 12 123C01, [Erratum: *PTEP* 2020, 029201 (2020)], 1808.10567.
- [6] M. Roney, *PoS ICHEP2020* (2021) 699.
- [7] Z. Liptak, M. Kuriki, and J. Roney in *Proc. IPAC'21*, no. 12, pp. 3799–3801, 2021.
- [8] C. M. Carloni Calame, C. Lunardini, G. Montagna, O. Nicosini, and F. Piccinini, *Nucl. Phys. B* **584** (2000) 459–479, hep-ph/0003268.
- [9] C. M. Carloni Calame, *Phys. Lett. B* **520** (2001) 16–24, hep-ph/0103117.
- [10] G. Balossini, C. M. Carloni Calame, G. Montagna, O. Nicosini, and F. Piccinini, *Nucl. Phys. B* **758** (2006) 227–253, hep-ph/0607181.
- [11] G. Balossini, C. Bignamini, C. M. C. Calame, G. Montagna, O. Nicosini, and F. Piccinini, *Phys. Lett. B* **663** (2008) 209–213, 0801.3360.
- [12] S. Jadach, B. Ward, and Z. Was, *Comput. Phys. Commun.* **130** (2000) 260–325, hep-ph/9912214.
- [13] S. Jadach, B. F. L. Ward, and Z. Was, *Phys. Rev. D* **88** (2013), no. 11 114022, 1307.4037.
- [14] A. B. Arbuzov, G. V. Fedotov, F. V. Ignatov, E. A. Kuraev, and A. L. Sibidanov, *Eur. Phys. J. C* **46** (2006) 689–703, hep-ph/0504233.
- [15] I. M. Nugent, “eeMC: Simulation of $e^+e^- \rightarrow \mu^+\mu^-(\gamma)$ and $e^+e^- \rightarrow \tau^+\tau^-(\gamma)$ Events”, preprint (4, 2022), 2204.02318.
- [16] R. Sadykov and V. Yermolchyk, *Comput. Phys. Commun.* **256** (2020) 107445, 2001.10755.
- [17] S. Bondarenko, Y. Dydyshka, L. Kalinovskaya, R. Sadykov, and V. Yermolchyk, *Phys. Rev. D* **102** (2020), no. 3 033004, 2005.04748.
- [18] A. B. Arbuzov, S. G. Bondarenko, L. V. Kalinovskaya, L. A. Rumyantsev, and V. L. Yermolchyk, *Phys. Rev. D* **105** (2022), no. 3 033009, 2112.09361.
- [19] F. Jegerlehner, *EPJ Web Conf.* **218** (2019) 01003, 1711.06089.
- [20] E. A. Kuraev and V. S. Fadin, *Sov. J. Nucl. Phys.* **41** (1985) 466–472.
- [21] O. Nicosini and L. Trentadue, *Phys. Lett. B* **196** (1987) 551.
- [22] A. Arbuzov, S. Bondarenko, L. Kalinovskaya, R. Sadykov, and V. Yermolchyk, *Symmetry* **13** (2021), no. 7 1256.